Mitt. Ges. Geol. Bergbaustud. Österr., **42**: 21-36, Wien 1999

Occurrence and mineral-chemistry of monazite and rhabdophane in the Lower and ?Middle Austroalpine tectonic units of the southern Sopron Hills (Austria)

by

Geza NAGY & Erich DRAGANITS

with 6 figures and 4 tables

Schlüsselwörter:
Unterostalpin
Monazit
Rhabdophan
Seltenerd-elemente
Mikrosonde

Keywords:
Lower Austroalpine
Monazite
Rhabdophane
Rare earth elements
Microprobe

Addresses of the authors:
Dr. GEZA NAGY
Laboratory for Geochemical Research
Hungarian Academy of Sciences
Budaorsi út 45
H-1112 Budapest
Hungary
E-mail: gnagy@sparc.core.hu

Mag. ERICH DRAGANITS
Institut für Geologie
Universität Wien
Althanstrasse 14
A-1090 Wien
Austria
E-mail: Erich.Draganits@univie.ac.at

Mitt. Ges. Geol. Bergbaustud. Österr.	42	S. 21-36	Wien 1999

Contents

Abstract

Electron microprobe (EMP) based investigations on the abundance, textural position, composition and genesis of accessory rare earth element (REE) minerals in the metamorphic rocks of the Sopron Hills were carried out. The most common of these minerals are monazite, rhabdophane (hydrous monazite-group mineral) and xenotime, whereas allanite and florencite (hydrous Al-phosphate mineral) are rare.
In the Sopron Hills two different lithological series exist. Generally monazite and xenotime is considerably more abundant in mica schists belonging to the Óbrennberg-Kaltes Bründl Series (ÓKB) than in the underlying Sopron Series. Florencite is restricted to leuchtenbergite-containing lithologies.
The compositions of monazite are similar in all samples. Monazite in the mica schists shows small but regular changes in the Y- and other heavy rare element (HREE-) contents. In the mica schists of the ÓKB-Series variations in Y and HREE content of monazite separate them into high-Y (1.15 - 1.85 wt.% Y_2O_3) and low-Y (< 0.65 wt.% Y_2O_3) monazites. In the Sopron Series there is a stronger scatter in the Y content of monazite, with no well-defined groups. Most of the monazites have moderately negative Eu anomalies. The ThO_2 contents of monazite vary within the samples, sometimes even within one grain. In both series the variations of the Th and Ca contents display a linear relationship, almost according to 2REE = Th + Ca.
Two distinct types of rhabdophane were found, which never occur in one single sample together. The more widespread Type 1 rhabdophane is either porous or consists of aggregates of small grains, often having the appearance of pseudomorphs. The oxide totals of the EMP-analyses range between 88.0 - 95.5 wt.%. Chemically, Type 1 rhabdophane contains excess Ca over Th, the Y and HREE contents are always higher than those of monazite in the same sample. The rare Type 2 rhabdophane is very similar to monazite in appearance, grain size and composition, but has 93.6 and 97.0 wt.% oxide totals. It has only been found in some mica schists.

Zusammenfassung

Die vorliegende Arbeit beschäftigt sich mit Mikrosonden-Untersuchungen der Häufigkeit, texturellen Position, Zusammensetzung und Genese von akzessorischen Seltenerd-Elemente (SEE) Mineralen in den Gesteinen des südlichen Ödenburger Gebirges. Die häufigsten dieser Minerale sind Monazit, Rhabdophan und Xenotim, während Allanit und Florenzit eher selten sind.
Das Kristallin des Ödenburger Gebirges kann bezüglich der Lithologien und Metamorphosegeschichte in zwei unterschiedliche Serien getrennt werden. Generell ist Monazit und Xenotim in den Glimmerschiefern der Óbrennberg-Kaltes Bründl Serie (ÓKB) viel häufiger als in jenen der Sopron Serie. Florenzit wurde nur in Leuchtenbergit führenden Gesteinen gefunden.
Die Monazite in den Glimmerschiefern der ÓKB Serie weisen deutliche Schwankungen in ihren Y- und schweren SEE-Gehalten auf, die eine Trennung in high-Y (1.15 - 1.85 wt.% Y_2O_3) und low-Y (< 0.65 wt.% Y_2O_3) Monazite ermöglichen. In den Proben der Sopron Serie streuen die Y-Gehalten ebenfalls relativ stark, ohne daß jedoch eine Trennung in unterschiedliche Gruppen möglich ist. Die Änderung der Th- und Ca-Gehalte der Monazite in beiden Serien zeigt eine lineare Beziehung ungefähr nach der Reaktion 2SEE = Th + Ca.
Es treten zwei unterschiedliche Typen von Rhabdophan auf, die nie gemeinsam in ein und derselben Probe beobachtet werden konnten. Der häufige Typ 1 Rhabdophan erscheint in back-scattered electron (BSE) Bildern porös oder aus vielen, sehr kleinen Einzelkörner aufgebaut zu sein, oft mit dem Erscheinungsbild einer Pseudomorphose. Die Summen der Mikrosonden Analysen in Oxydgewichten liegen zwischen 88.0 und 95.5 %. In seiner Zusammensetzung enthält Typ 1 Rhabdophan deutlich mehr Ca als Th, zusätzlich ist der Gehalt an Y und den schweren SEE immer höher als in den Monaziten in denselben Proben.
Der seltene Typ 2 Rhabdophan ist Monazit in Aussehen, Korngröße und Zusammensetzung sehr ähnlich, im Unterschied zu diesem liegen die Summen der Mikrosonden Analysen in Oxydgewichten jedoch zwischen 93.6 und 97.0 %. Typ 2 Rhabdophan findet sich nur in einigen wenigen Glimmerschiefer. In seiner chemischen Zusammensetzung fällt der geringere Gehalt an CaO bezüglich ThO_2 auf.

1. Introduction

During extensive prospecting for REE and Th in the Hungarian part of the Sopron Hills FAZEKAS et al. (1975) mentioned the occurrence of monazite, florencite, thorite and thorianite in certain lithologies. In a continuation of

this survey, KIESL et al. (1983) investigated samples from compareable lithologies in the Lower Austroalpine tectonic unit in the area of Birkfeld (Styria, Austria). In their studies they investigated the bulk rare earth element (REE) content of both the rocks and the heavy mineral fraction. BERNHARD et al. (1998) carried out electron microprobe (EMP) age determination on monazite of Austroalpine basement rocks in the Fischbacher Alpen.
This work concentrates on the abundance, textural position, composition and genetic aspects of the accessory REE-minerals in the Sopron Hills (Fig. 1). The most widespread of these minerals are monazite, rhabdophane and xenotime, while allanite and florencite are less abundant.
This paper summarises EMP-analysis of about 75 monazite and 60 rhabdophane grains in 19 samples (Tab. 2), emphasising the significant differences in chemical compositions, and attempts to relate them to the conditions of rock formation. NAGY & ÁRKAI (1999) have carried out similar investigations on rocks in the Hungarian part of the Sopron Hills; their results are compared in the discussion. When ever possible we used mineral abbreviations after KRETZ (1983), exceptions are leuchtenbergite (Lbg), rhabdophane (Rha) and sericite (Ser).

Monazite is a monoclinic Ce-phosphate mineral with the ideal formula $CePO_4$, where Ce can be replaced by the other light rare earth elements (LREE) in any proportion. The co-ordination number for REE is 9, which is the site in the lattice favoured by LREE with bigger ionic radii. Usually a few percent of La-Sm, Gd, and some tenth of a percent of Eu and heavier REE including Y are present. The proportions of the individual REE may differ depending on the conditions of formation. Moreover, monazite often contains a few percent ThO_2 (may be over 10 wt.%), less U, Ca and some Si. The last two elements balance the charge differences of the REE and actinides according to the following reactions:

$$2REE^{3+} = (Th,U)^{4+} + Ca^{2+} \quad (1)$$

or

$$REE^{3+} + P^{5+} = (Th,U)^{4+} + Si^{4+} \quad (2)$$

Chemically related minerals are: (1) Xenotime, YPO_4, tetragonal, with a REE co-ordination number of 8, so that it prefers the HREE with smaller ionic radii; (2) Cheralite, $(Ce,Ca,Th)\cdot(P,Si)O_4$, is a member of the monazite $CePO_4$ - brabantite $CaTh(PO_4)_2$ series, isostructural with monazite (HUGHES et al. 1995); (3) Rhabdophane, $CePO_4\cdot H_2O$ or $\cdot nH_2O$, hexagonal (details see below); (4) Brockite, $(Ce,Th,Ca)PO_4\cdot H_2O$ or $\cdot nH_2O$, hexagonal, a member of the rhabdophane group.

Formation of monazite
Monazite is a common accessory mineral in acidic intrusive rocks, but it can also be formed during metamorphism, although little is known about the formation of metamorphic monazite (GRAUCH 1989, AKERS et al. 1993, PAN 1997). The sources of REE and P in metamorphic monazite are presumably the major minerals or former accessory REE minerals of the original rock (KIESL et al. 1983, LANZIROTTI & HANSON 1996), although migration of REE may also occur (SAWKA et al. 1986).
For monazite formation during prograde metamorphic processes, SAWKA et al. (1986) described the formation of hydrous REE-phosphates, like rhabdophane and florencite, $CeAl_3(PO_4)_2(OH)_6$, during weathering from aqueous solutions on the weathered surface of apatite grains. At elevated temperatures during subsequent metamorphism, they lose water and change to monazite. In this process, rhabdophane may quickly be transformed to monazite by mechanical strain, even at room temperature (HIKICHI et al. 1991) or by simple heating in air at 400 °C (VLASOV 1964). However, experiments by AKERS et al. (1993) showed that rhabdophane completely dehydrates to monazite at H_2O pressures of 0.05 - 0.20 GPa in excess of 200 °C and the presence of a graphite-methane oxygen buffer. Due to this low stability field, they precluded rhabdophane from being an immediate precursor to neoformed monazite in lower amphibolite-grade metamorphic sequences.
LANZIROTTI & HANSON (1996) mentioned idioblastic monazite in greenschist grade rocks, which formed by disintegration and recrystallisation of former monazite with different compositions.
The shape and composition of monazite are dependent on the metamorphic conditions where they have been formed. FRANZ et al. (1996) described monazite and xenotime in a metapelite-psammite series formed during greenschist to granulite grade regional metamorphism. Monazite grains that formed at low temperature are small and amoeboidal. With increasing metamorphic grade the grains tend to become bigger and more regular and the variation of La_2O_3 - Sm_2O_3 decreases whilst the average content and scatter of Y_2O_3 increases. Concerning ThO_2 and CaO no general dependency on metamorphic grade was observed. Based on the variations of REE-contents in monazite, HEINRICH et al. (1997) and GRATZ & HEINRICH (1997, 1998) proposed an empirical geothermometer.

Rhabdophane is a hexagonal water-containing phosphate mineral. The composition and its X-ray diffractogram are very similar to monazite (VLASOV 1964). The major difference is that rhabdophane contains small irregular channels in which water occurs (MOONEY 1950). Thus its ideal formula is given as $CePO_4\cdot H_2O$ (VLASOV 1964, CLARK 1984, CESBRON 1989, JONES et al., 1996) or $CePO_4\cdot nH_2O$, n = 0 - 0.5, according to STRUNZ (1970) and BURT (1989). The ideal water content is 7.1 wt.% with 1 H_2O and 3.7 wt.% with 0.5 H_2O.
However, in analyses of rhabdophane the water content varies considerably. VLASOV (1964) reported water contents between 6.0 and 10.6 wt.%, with a mean about 7.4 wt.%. BOWLES & MORGAN (1984) described rhabdophane from Cornwall containing 7.9 wt.% water, determined by differential thermal analysis (DTA).

Formation of rhabdophane
Models for rhabdophane formation involve a cycle of weathering - transport in aqueous solutions - fixation processes (SAWKA et al. 1986, BANFIELD & EGGLETON 1989), with Ce strongly fractionationed during the formation of rhabdophane, with the concentration of other REE not changing much. BRAUN et al. (1990) described similar

processes in soils originating from syenites and gneisses with a strong Ce fractionation and an enrichment of HREE in the aqueous phase.

Rhabdophane easily looses water during heating and transforms to monazite. From the experiments mentioned above, it can be concluded that rhabdophane is stable only at low temperatures and, presumably, among oxidising conditions. AKERS et al. (1993) defined the upper stability limit of rhabdophane at 200 °C with H_2O pressures of 0.05 - 0.20 GPa.

2. Geological background

The crystalline rocks of the Sopron Hills represent one of the easternmost outcrops of the Austroalpine basement. In spite of poor outcrop, the multiphase metamorphic and tectonic history, including relatively good preservation of pre-Alpine mineral assemblages, has attracted a lot of research in recent years.

Two different lithological series have been distinguished. Mica schists and gneisses with abundant biotite, thin quartz-layers, coarse grained pegmatites and a weak foliation occur mainly in the uppermost levels of the crystalline series. They have been differentiated from markedly foliated, chlorite- and garnet-rich, diaphthoritic mica schists in close contact with orthogneisses (Fig. 1). The former lithological group represents the Óbrennberg-Kaltes Bründl Series (ÓKB Series), the latter the Sopron Series (DRAGANITS 1998). These two series also differ in the abundance and composition of their accessory REE-minerals (Tabs. 1 and 2). Major element and trace element discrimination diagrams indicate that shales with an island-arc-signature are the most probable protoliths for the mica schists of both series (DRAGANITS 1998).

The ÓKB Series mainly comprises biotite-sericite-chloritoide-garnet-schists and biotite-sericite-sillimanite-schists. Biotite-andalusite-sillimanite schists, which represent the best-preserved pre-Alpine rocks in this area, have been found in a few places (DRAGANITS 1996). Kyanite-leuchtenbergite-muscovite quartzites also occur in this series.

The Sopron Series is characterised by monotonous diaphthoritic mica schists with varying quartz-contents and numerous rectangular to rhomboic pseudomorphs, probably after staurolite. These pseudomorphs contain either sericite, or sericite with chloritoid, or chloritoid with kyanite, depending on the bulk chemistry and the degree of Alpine overprint; relicts of staurolite within these pseudomorphs are scarce. Leucocratic, moderately foliated, medium-grained gneisses are associated with these mica schists. The occurrence of Ms-Lbg-schists (Leukophyllites) and Ky-Lbg-(Ms) quartzites has been related to metasomatic processes along Alpine shear zones (HUBER 1993, DEMÉNY et al. 1997).

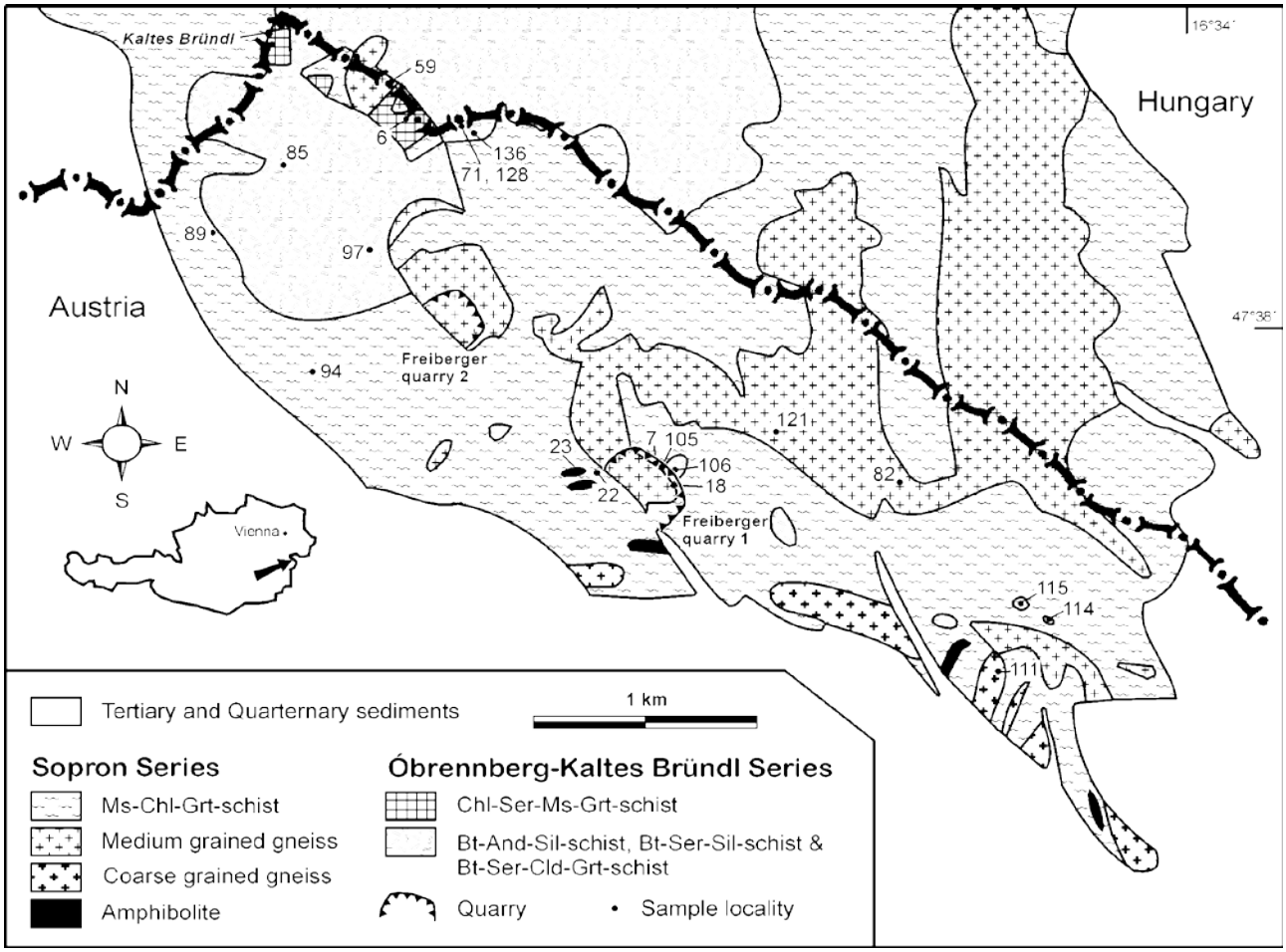

Fig. 1: Geological map of the southern part of the Sopron Hills with the sample locations. Simplified after DRAGANITS (1996). For space reasons, the samples are noted with the continuous sample number without years-extension.

In the very southern part of the crystalline massif, these mica schists contain several small bodies of garnet-amphibolite, most highly deformed, but some with a relict meta-gabbroic texture. Characteristic, coarse-grained orthogneiss („Grobgneis") without any transitions to the medium-grained gneisses only occurs south of the amphibolites (Fig. 1).

The occurrence of coarse-grained gneisses and meta-gabbros in only the southern part of the Sopron Hills is noticeable, and the two-fold division of the region presented by DRAGANITS (1996) might be modified to a three-fold one, in which the above mentioned lithological association in the south is separated from the rest of the Sopron Series, representing the Grobgneis Complex *senso stricto*.

Since the crystalline unit forms an inlier surrounded by Tertiary sediments, correlation with comparable lithologies to the west remains a matter of discussion. The lithologies of the ÓKB Series possibly belong to the Middle Austroalpine tectonic unit and are probably correlatives of the „Strallegger Gneis" in the area of Birkfeld, Styria. The majority of the mica schist of the Sopron Series are comparable with the „Tommer Schiefer" in the same area (SCHWINNER 1935, KOLLER & WIESENEDER 1981, BERKA et al. 1998).

The ÓKB and Sopron Series also differ in their metamorphic history. The Sopron Series shows evidence of two amphibolite-grade metamorphic events, while the ÓKB Series displays an even more complex history, in which remnants of staurolite included in andalusite indicate an amphibolite-grade metamorphic event before the main andalusite, sillimanite and biotite forming event, followed by a final amphibolite-grade metamorphic event with kyanite, staurolite, chloritoid and garnet growth (LELKES-FELVÁRI & SASSI 1984, KISHÁZI & IVANCSICS 1985). Preliminary isotope age determinations on samples from the Sopron Hills as well as on similar rocks in the Eastern Alps point to a Variscan age for the first event, followed by a Permian low P/high T-event and a final Alpine overprint (DRAGANITS 1996, BERKA et al. 1998, SCHUSTER et al. 1998, BALOGH & DUNKL 1998).

The relict nature of minerals from the first event makes P/T estimations difficult; the conditions of the pre-Alpine high T metamorphic event in the ÓKB Series are estimated at 650 °C and 3 - 5 kbar (DRAGANITS 1996). The P/T conditions of the Alpine overprint range from greenschist to lower amphibolite facies.

There is relatively good agreement among recent publications, concerning the Alpine metamorphic event in the Sopron Series, correlating with the data of FARYAD & HOINKES (1998) from the Grobgneis Complex. DRAGANITS (1996) used phengite barometry and mineral assemblages to define 0.95 ± 0.15 GPa at 550 ± 30 °C. TÖRÖK (1996) applied phengite barometry and fluid inclusions data and obtained 1.2 GPa at 450 - 500 °C, while 1.3 GPa and 560 ± 30 °C have been suggested by DEMÉNY et al. (1997), using phengite barometry and quartz oxygen isotope fractionation.

3. Methods

Based on optical examination of thin-sections from 141 rock samples (DRAGANITS 1998) a representative selection of each lithology, with the best preserved samples and those which appeared to be rich in REE accessory-minerals were taken for further EMP investigations (Tab. 1). For sample localities see Fig. 1.

The accessory minerals were identified by electron microprobe (EMP) in thin- or thick-sections. The microprobe work was done by a JCXA-733 (JEOL) instrument of the Laboratory for Geochemical Research in Budapest, equipped with 3 wavelength dispersive spectrometers (WDS) and an energy dispersive spectrometer (EDS). The whole surface of the sections were examined by backscattered electron (BSE) image, which was set so that all grains of rutile or heavier minerals with *c.* 10 µm diameter or apatite with *c.*50 µm diameter could be detected. Most of the minerals were identified by EDS spectra; in this way the heavier accessory minerals (e. g. garnet) were reliably identified, although some light ones (e. g. tourmaline) might have been overlooked. This method enabled us to count the number of monazite grains or rhabdophane aggregates and roughly estimate the abundance of these minerals.

Quantitative mineral analyses were done by WDS-s, using a method described by NAGY (1993), in which a parabola fitted to peakless ranges of the X-ray spectra determines

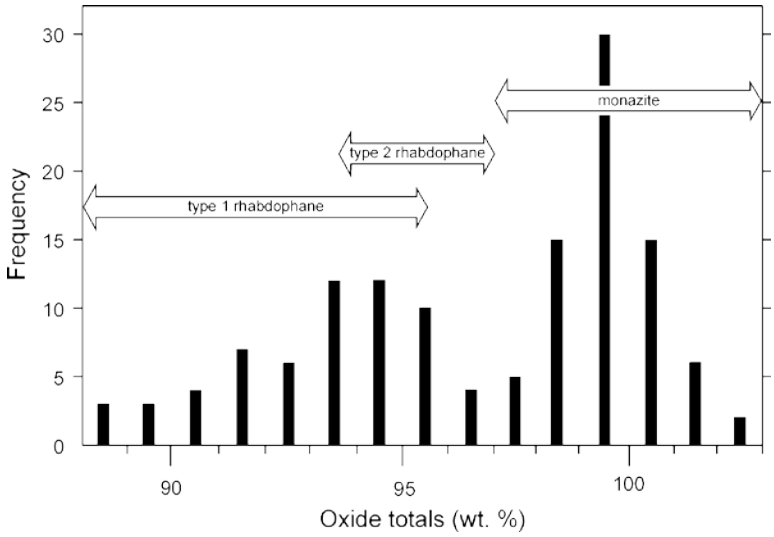

Fig. 2: Frequency distribution diagram of oxide totals from 134 EMP-analyses. While there is a good separation between monazite and rhabdophane (in general), the frequency distribution between Type 1- and Type 2 rhabdophane is overlapping between 93.6 - 95.5 %. Thus, the differentiation between the two types of rhabdophanes are mainly based on their appearance and their Ca/Th-ratios.

Mineral assemblage of the analysed samples

Sample	Lithology	Series	Qtz	Ms	Bt	Pl	Kfs	AluSil	Grt	Chl	Cld	Lbg	Pg	St	Tur	Mnz	Rha1	Rha2	Xen	Ap	Zrn	Rt	Ilm	FeOx	other minerals, notes
NM92-71	Bt-And-Sil schist	ÓKB	+	+	++	+	+	+	+	-	-	-	-	-	+	++	+	-	+	-	+	-	+	+	Rha on Mnz
NM93-97	Bt-And-Sil schist	ÓKB	+	+	++	+	-	++	-	-	+?	-	-	+?	-	++	-	-	+	+	+	+	+	-	Jarosite
NM93-106	Bt-And-Sil schist	ÓKB	+	+	++	+	+	++	(+)	(+)	-	-	-	-	-	++	+	-	++	+	++	+	+	+	Aln
NM93-114	Bt-And-Sil schist	ÓKB	++	++	++	+	+	+	-	-	-	-	-	+	-	++	-	+	++	-	-	-	+	+	
NM93-115	Bt-And-Sil schist	ÓKB	+	++	++	+	+?	+	-	-	+?	-	-	+?	-	-	-	++	+	-	+	-	+	+	
NM93-128	Bt-And-Sil schist	ÓKB	++	++	+	+	+	++	+	-	-	-	-	+	-	++	-	+	+	+	+	-	+	-	
NM92-6	Chl-Ser-Grt schist	ÓKB	+	+	-	+	-	-	+	+	-	-	+	-	-	-	++	-	-	+	+	-	++	-	
NM93-105	Chl-Ser-Grt schist	ÓKB	+	+	+	+	-	-	+	+	-	-	-	-	-	++	(+)	-	+	-	+	-	+	+	Crn, Py
NM93-136	Grt-Bt gneiss	ÓKB	++	+	++	(+)	-	-	++	-	-	-	-	-	-	+	+	-	-	-	++	-	+	+	
NM92-7	Ms-Chl-Tur schist	SS	++	++	-	-	-	-	-	+	-	-	-	-	++	+	+	-	-	-	+	+	++	-	Jarosite
NM92-18	Ms-Chl-Grt schist	SS	+	++	-	-	-	-	+	++	+	-	-	-	-	-	+	-	-	+	+	+	+	-	Py, Ccp, Bravoite
NM92-22	Ms-Chl-Grt-St schist	SS	+	+	-	-	-	++	+	+	+	-	+	++	-	-	-	++	-	+*	+	+	-	+	Ti-Mag
NM92-59	Ms-Chl-Grt-Bt schist	SS	++	++	+	+	-	-	+	+	-	-	-	-	+	i	++	-	-	+	++	-	++	+	Py; Mnz in Grt
NM93-82	medium ortho-gneiss	SS	++	++	+	+	++	-	(+)	-	-	-	-	-	-	-	++	-	-	+	+	+	-	+	Pb-Fe-P-S mineral
NM93-121	medium ortho-gneiss	SS	++	++	+	+	++	-	+	-	-	-	-	-	-	i	+	-	-	+	+	+	+	-	Mnz in Ap only
NM93-94	coarse ortho-gneiss	SS	++	+	+	++	+	-	+	-	-	-	-	-	-	-	+?	-	-	+	+	+	-	+	Ce-oxide, Brockite, Aln
NM93-111	coarse ortho-gneiss	SS	++	+	+	++	+	-	+	-	-	-	-	-	-	-	+	-	-	+	+	+	-	-	
NM93-85	Leucophyllite	SS	++	++	-	-	-	-	-	-	-	++	-	-	-	++	-	-	+	+*	+	+	-	-	Florencite
NM93-89	Ky-Lbg quartzite	SS	++	+	-	-	-	++	-	-	-	++	-	-	-	+	-	-	+	(+)*	++	++	-	-	Few Ap with little Cl

(+) = rare, + = common, ++ = abundant, i = inclusions, * = Cl-containing apatite

Tab. 1: Summary of the analysed samples, their affiliation to the lithological series and the mineralogical contents.

Summary of analysed monazite and rhabdophane

Sample	Total #Mnz	Number of monazite analyses low-Y Mnz 0-0.65%	0.65-1.15%	high-Y Mnz 1.15-1.85%	>1.85%	Total #Rha	No. of Rha analyes Type 1 Rha	Type 2 Rha
NM92-71	40	8	–	–	–	5	3	–
NM93-97	50	4	–	6	1^+	–	–	–
NM93-106	70	–	–	5	–	15	3	–
NM93-114	100	1^+	1	8	–	5	–	1
NM93-115	–	–	–	–	–	150	–	8
NM93-128	75	10	–	–		20	–	6
NM92-6	–	–	–	–	–	40	5	–
NM93-105	50	9	–	–	–	–	–	–
NM93-136	30	5	–	–	–	25	1	–
NM92-7	1	–	1	–	1^+	20	2	–
NM92-18	–	–	–	–	–	25	–	–
NM92-22	–	–	–	–	–	100	–	7
NM92-59	2	–	–	2	–	50	9	–
NM93-82	–	–	–	–	–	30	5	–
NM93-121	6	–	4^+	–	–	25	3	–
NM93-94	–	–	–	–	–	–	–	–
NM93-111	–	–	–	–	–	15	3	–
NM93-85	80	1	2^+	$3(1^+)$	1^+	–	–	–
NM93-89	33	1	2	2	–	–	–	–

$^+$ = Eu/Eu* < 0.35

Tab. 2: Estimated number of monazite, Type 1 (clusters) and Type 2 rhabdophane per thin-section, >10 mm in size respectively, and number of analysed REE-minerals per sample and their affiliation to specific mineral groups.

the backgrounds for the analytical peaks of lanthanides. Analytical conditions were set at 20 kV accelerating voltage; 40 nA electron current, 5 times 4 s counting time; the electron beam was opened to 6 or 3 µm diameter (depending on the grain size), focussed only if absolutely necessary. Lines used for analysis were: K_α for light elements (Ca, P, Si); L_α for most REE; L_β for Pr; M_α for Th; M_β for U. Pre-measured correction factors were applied to eliminate the effect of Pr-Eu, La-Gd, Ce-Gd and Th-U line overlaps. The following standards were used: glasses of DRAKE & WEILL (1972) for REE, Durango apatite for P and Ca from E. JAROSEWICH (Smithsonian Inst., Washington); oxide for Th from C. M. TAYLOR (Stanford, Calif.); URuSi for U from T. GORTMÜLLER (Kammerlingh Onnes Lab., Leiden). Rough data were corrected by conventional ZAF method. The points of analyses were set on BSE image to eliminate inclusions etc. The uncertainties (calculated from two standard deviation, 2σ, i.e. with 95 % confidence level) and detection limits of a representative monazite analysis can be seen in Tab. 3. The standard deviation of the oxide totals of 75 monazite analyses is 1.0 wt.%, (Fig. 2), slightly higher than estimated in Tab. 3 (0.86 wt.%), their average is 99.6 wt.%. The difference indicates that the uncertainties may be slightly (*c.* 1.2 times) higher for the majority of analyses then given in Tab. 3, or it may originate from unmeasured components. Monazite and rhabdophane, which have similar EDS-spectra, were distinguished by their measured oxide totals (Σ), presuming that the difference from Σ = 100.0 wt.% reflects the water content. The monazite-rhabdophane boundary was set at Σ = 97.0 wt.%, except for small inclusions (Fig. 2).

The analytical results have been recalculated to ionic numbers for unit cells containing 16 oxygen. The Eu-anomaly is characterised by the Eu/Eu* quotient, where Eu is the measured value, and Eu* is calculated from Sm and Gd by straight-line interpolation on a logarithmic chondrite-normalised abundance diagram (HENDERSON 1984: 9). Chondrite values of TAYLOR & MCLENNAN (1985: 298) were used. Calculations were done by the following formula:

$$Eu^* = Eu(chond) \cdot \sqrt{\frac{Sm}{Sm(chond)} \cdot \frac{Gd}{Gd(chond)}}$$
$$= const \cdot \sqrt{Sm \cdot Gd} \qquad (3)$$

4. Results

The main, minor and accessory minerals of the samples have been investigated by optical microscopy and EMP (summarised in Tab. 1). The approximate number of monazite and Type 2 rhabdophane grains bigger than 10 µm, as well as clusters of small (< 10 µm) grains of Type 1 rhabdophane per thin-section are shown in Tab. 2. As a general trend within the two series, monazite is considerable more abundant in most of the mica schists of the ÓKB Series

Monazite analyses

Sample	NM92-71 Low-Y ÓKB Series	NM93-97 (rim) Low-Y ÓKB Series	NM93-97 (core) High-Y ÓKB Series	NM93-97 Atypical ÓKB Series	NM93-115 Low-Y ÓKB Series	NM92-59 Incl. in Grt Sopron Series	NM93-89 Sopron Series	NM93-121 Incl. in Ap Sopron Series	NM92-59 ±Δ	NM92-59 Detect. limit
Y_2O_3	0.29	0.55	1.57	2.38	0.21	1.38	0.65	1.08	±0.22	0.03
La_2O_3	14.38	14.19	13.07	10.21	13.50	13.03	13.91	11.89	±0.84	0.15
Ce_2O_3	29.53	30.25	28.33	22.72	30.31	29.00	29.08	27.48	±1.32	0.12
Pr_2O_3	2.85	3.09	2.73	2.27	3.11	2.78	3.08	2.56	±0.26	0.17
Nd_2O_3	11.83	12.37	11.31	9.51	12.80	11.53	12.11	10.75	±0.42	0.11
Sm_2O_3	2.11	2.21	2.23	1.92	2.31	2.19	2.28	2.07	±0.16	0.08
Eu_2O_3	0.42	0.40	0.32	0.18	0.50	0.29	0.35	0.11	±0.08	0.11
Gd_2O_3	1.76	1.64	1.84	1.76	1.44	1.74	1.82	1.41	±0.14	0.11
Tb_2O_3	0.12	0.10	0.17	0.24	0.11	0.15	0.12	0.13	±0.08	0.10
Dy_2O_3	0.19	0.43	0.63	0.86	0.17	0.60	0.41	0.37	±0.06	0.09
Er_2O_3	n.d.	n.d.	n.d.	0.22	n.d.	n.d.	n.d.	n.d.	±0.08	0.10
CaO	0.74	0.76	1.35	2.89	0.66	1.02	0.62	2.55	±0.02	0.01
ThO_2	4.95	4.33	5.24	14.16	3.39	6.43	2.75	6.98	±0.18	0.03
UO_2	0.46	0.46	1.65	1.14	0.46	0.40	0.74	0.38	±0.12	0.10
SiO_2	0.15	0.21	0.00	0.11	0.02	0.31	0.06	0.29	±0.06	0.02
P_2O_5	29.88	29.64	30.15	30.52	30.51	29.09	29.81	29.51	±0.30	0.02
Total	99.60	100.62	100.64	101.15	99.51	99.97	97.79	97.58	±1.72	
Ionic numbers based on 16 Oxygens										
Y	0.024	0.046	0.130	0.195	0.017	0.116	0.055	0.091	±0.019	
La	0.837	0.823	0.752	0.580	0.779	0.762	0.818	0.695	±0.049	
Ce	1.706	1.741	1.618	1.281	1.737	1.684	1.698	1.596	±0.077	
Pr	0.164	0.177	0.155	0.127	0.177	0.161	0.179	0.148	±0.015	
Nd	0.667	0.694	0.630	0.523	0.716	0.653	0.690	0.609	±0.024	
Sm	0.115	0.120	0.120	0.102	0.125	0.120	0.125	0.113	±0.009	
Eu	0.023	0.021	0.017	0.009	0.027	0.016	0.019	0.006	±0.004	
Gd	0.092	0.085	0.095	0.090	0.075	0.092	0.096	0.074	±0.007	
Tb	0.006	0.005	0.009	0.012	0.006	0.008	0.006	0.007	0.004	
Dy	0.010	0.022	0.032	0.043	0.009	0.031	0.021	0.019	±0.004	
Er	-	-	-	0.011	-	-	-	-	±0.003	
Ca	0.125	0.128	0.226	0.477	0.111	0.173	0.106	0.433	±0.003	
Th	0.178	0.155	0.186	0.496	0.121	0.232	0.100	0.252	±0.006	
U	0.016	0.016	0.057	0.039	0.016	0.014	0.026	0.013	±0.004	
Si	0.024	0.033	-	0.017	0.003	0.049	0.010	0.046	±0.010	
P	3.991	3.944	3.981	3.981	4.044	3.907	4.024	3.962	±0.040	
Σ	7.951	8.012	8.008	7.988	7.961	8.021	7.974	8.066	±0.107	
Eu/Eu*	0.66	0.64	0.48	0.30	0.83	0.45	0.52	0.20	±0.130	

n.d. = measured values below the detection limit

Tab. 3: Selected EMP-analyses of monazite. Values represent oxide wt.%. Monazites are discriminated by their Y-contents in high-Y- (1.15-1.85% Y_2O_3) and low-Y monazites (<0.65% Y_2O_3). Measurements errors and detection limits calculated on sample NM92-59.

than in the Sopron Series. Most of the monazites show xenoblastic shape, idioblastic grains are rare. Chemical differences could not be related to different shapes. Rhabdophane is always xenoblastic.

Two types of rhabdophanes were recorded, easily distinguished by their appearance (Fig. 4c, d and f), Ca/Th ratios, and different oxide totals (Fig. 2); they have never been found in one sample together. Monazite and Type 2 rhabdophane often appear as mono-crystalline grains, up to 100 mm large, whereas Type 1 rhabdophane mainly occurs in clusters showing the habit of a pseudomorph after a former REE-mineral. Xenotime occurs in most mica schists of the

Rhabdphane analyses

Sample	**NM92-6** Type 1 ÓKB Series	**NM92-71** Type 1 ÓKB Series	**NM92-115** Type 2 ÓKB Series	**NM93-128** Type 2 ÓKB Series	**NM93-22** Type 2 Sopron Series	**NM93-59** Type 1 Sopron Series	**NM92-121** Type 1 Sopron Series
Y_2O_3	1.60	2.83	0.62	0.32	0.06	1.75	3.09
La_2O_3	11.05	10.91	13.52	13.61	14.47	11.03	10.18
Ce_2O_3	24.22	20.22	29.46	28.95	29.23	23.25	22.91
Pr_2O_3	2.47	2.21	2.89	3.04	2.75	2.20	2.55
Nd_2O_3	9.35	8.80	11.44	11.94	11.49	9.01	9.30
Sm_2O_3	1.89	1.71	2.21	2.35	1.95	1.49	2.09
Eu_2O_3	0.40	0.47	0.39	0.40	0.50	0.38	0.33
Gd_2O_3	1.53	2.02	1.68	1.57	1.21	1.42	1.69
Tb_2O_3	0.16	0.16	0.19	0.11	n.d.	0.14	0.17
Dy_2O_3	0.56	0.92	0.36	0.24	0.16	0.56	0.70
Er_2O_3	0.13	0.39	n.d.	n.d.	n.d.	0.18	0.22
CaO	4.76	3.90	0.38	0.59	0.58	5.47	4.63
ThO_2	3.89	9.01	1.48	2.98	2.72	8.16	1.85
UO_2	0.39	0.59	0.48	0.47	0.61	0.36	0.56
SiO_2	0.16	0.64	0.02	0.15	0.05	0.07	0.27
P_2O_5	28.96	27.48	29.92	28.25	29.45	28.62	28.77
Total	91.61	92.49	95.06	95.03	95.24	94.11	89.39
Ionic numbers based on 16 Oxygens							
Y	0.139	0.250	0.053	0.028	0.005	0.151	0.271
La	0.665	0.669	0.806	0.833	0.869	0.658	0.618
Ce	1.446	1.231	1.743	1.758	1.742	1.378	1.381
Pr	0.147	0.134	0.170	0.184	0.163	0.130	0.153
Nd	0.545	0.522	0.660	0.708	0.668	0.521	0.547
Sm	0.106	0.098	0.123	0.134	0.109	0.083	0.119
Eu	0.022	0.027	0.022	0.023	0.028	0.021	0.019
Gd	0.083	0.111	0.090	0.086	0.065	0.076	0.092
Tb	0.009	0.009	0.010	0.006	-	0.007	0.009
Dy	0.029	0.049	0.019	0.013	0.008	0.029	0.037
Er	0.007	0.020	-	-	-	0.009	0.011
Ca	0.832	0.695	0.066	0.105	0.101	0.949	0.817
Th	0.144	0.341	0.054	0.113	0.101	0.301	0.069
U	0.014	0.022	0.017	0.017	0.022	0.013	0.021
Si	0.026	0.106	0.003	0.025	0.008	0.011	0.044
P	3.999	3.868	4.095	3.968	4.059	3.922	4.010
Σ	8.217	7.901	7.934	8.005	7.950	8.260	8.221
Eu/Eu*	0.71	0.77	0.62	0.63	0.99	0.80	0.53

n.d. = measured values below the detection limit

Tab. 4: Selected EMP-analyses of rhabdophane. Values represent oxide wt.%. Note the high Y-contents and the low oxide totals of Type 1 rhabdophane compared with those of Type 2 rhabdophane.

ÓKB Series and in leuchtenbergite-bearing rocks of the Sopron Series.

Chondrite-normalized REE patterns are plotted for representative averages of differentiated groups. In most cases, however, they are very similar (Fig. 3). Analyses are individually plotted in the Eu/Eu* *vs.* Y_2O_3 and CaO *vs.* ThO_2 fields (Fig. 5; 6). Selected analyses are given in Tabs. 3 and 4, the total data set is available upon request free of

charge from the first author.

Óbrennberg-Kaltes Bründl Series

Biotite-andalusite-sillimanite schists

Six samples were investigated. All contain abundant LREE-phosphate minerals (Tab. 2) and some xenotime, which is usually enclosed in biotite.

Monazite was found in 5 samples. Most monazites are inclusions in andalusite and biotite or can be found at the boundary between biotite and andalusite (Fig. 4a and b). In sample NM93-97, monazite seems to overgrow small xenotime grains enclosed in biotite (Fig. 4b). Some grains are idioblastic, most are xenoblastic and have a rhabdophane rim in places. Texturally, many of the monazites seem to be older than, or contemporaneous with the andalusite, thus belonging to the first staurolite producing or the second andalusite/biotite-producing metamorphic overprint (see also BERNHARD et al. 1998).

The compositional range of monazite is usually small. The most obvious uniform changes can be observed in the Y contents, which are rather similar within single samples, independent of the textural position, but vary between different samples. The variations in the Y-content enable a distinction between two chemical groups of monazite; high-Y (1.15-1.85 wt.% Y_2O_3) and low-Y monazites (< 0.35 wt.% Y_2O_3). In the plot Eu/Eu* *vs*. Y_2O_3 there is a well-defined gap in the Y-contents between the two groups (Fig. 5a and b). Samples NM93-97, NM93-106 and NM93-114 contain high-Y monazites, whereas NM93-128 and NM92-71, similarly with the chlorite-sericite-garnet schist of NM93-105, have low-Y monazites (Fig. 5a and b, Tab. 2).

NM93-97 contains a chemically zoned monazite, intercalated with biotite and andalusite. Its central part has a high Y_2O_3 content (1.57 wt.%), similar to other big grains (1.15 - 1.55 wt.%), whereas the rim and some small grains have only 0.40 - 0.66 wt.% Y_2O_3. Additionally, a few monazites have Y-contents different from both groups, such as a monazite inclusion in biotite and, being in vicinity of xenotime (Fig. 4b), with unusually high Y content (2.38 wt.%). Another grain, poor in Y, was found in sample NM93-114. Monazite usually displays moderately negative Eu-anomalies (Eu/Eu* = 0.50 - 0.75), except for monazites with atypical Y-contents, which show unusually strong negative Eu-anomalies.

The Th and Ca contents change in a linear relationship (Fig. 6a), nearly according to formula (1). Thorium varies significantly, which seems to be independent of changes in the concentration of Y and REE (Tab. 3).

Rhabdophane shows two varieties, in both appearance and composition. Type 1 rhabdophane seems to be porous or built up of small grains. It was found as clusters of small, irregular grains at the corroded rims of some monazite in sample NM92-71 (Fig. 4c) or independently of monazite in NM92-71 and in NM93-106. Chemically, it is characterised by a high Ca content, which is definitely higher than necessary to compensate for Th and U entry according to reaction (1). This makes its energy dispersive spectrometer (EDS) spectrum different from the monazite spectrum. Usually, the Y and HREE-contents are also high compared to monazite, which makes the chondrite normalised pattern distinctive (Fig. 3a and b). The oxide totals range between 88.0 - 95.5 wt.%.

Type 2 rhabdophane is very similar to monazite in its appearance and composition. In BSE pictures they show slightly lower brightness compared with monazite (Fig. 4d). Their compositions are quite similar, except for the oxide totals, which are around 100.0 wt.% for monazite and around 95.0 wt.% for Type 2 rhabdophane (Tab. 3 and 4).

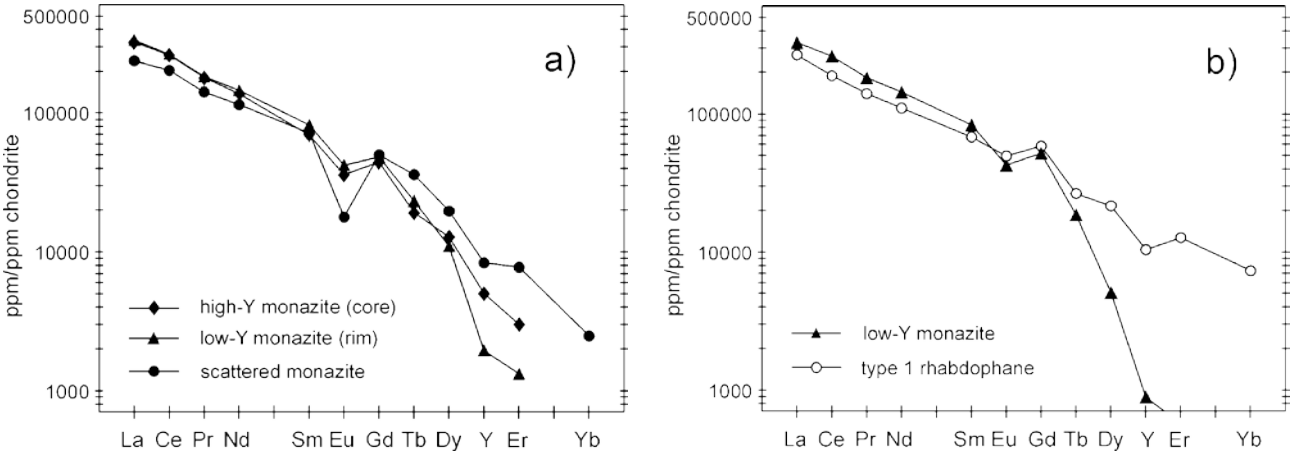

Fig. 3: Chondrite normalised REE patterns of monazite and rhabdophane in selected Bt-And-Sil schists (ÓKB series) **a)** Monazites of sample NM93-97: observe the differing values of the Eu-anomalies of high- and low-Y monazites and one scattered data point of monazite. **b)** Monazite and Type 1 rhabdophane of sample NM92-71.

Chlorite-sericite-garnet schists

Sample NM93-105 contains many monazite grains. They have irregular boundaries, seem to be corroded, and often appear in groups; some are enclosed in biotite or garnet. Some of the monazites, especially the inclusions in garnet, show thin rhabdophane rims. Their compositions are rather uniform, similar with the low-Y monazite of some biotite-andalusite-sillimanite schist. Few xenotime grains, included in garnet, were also found.

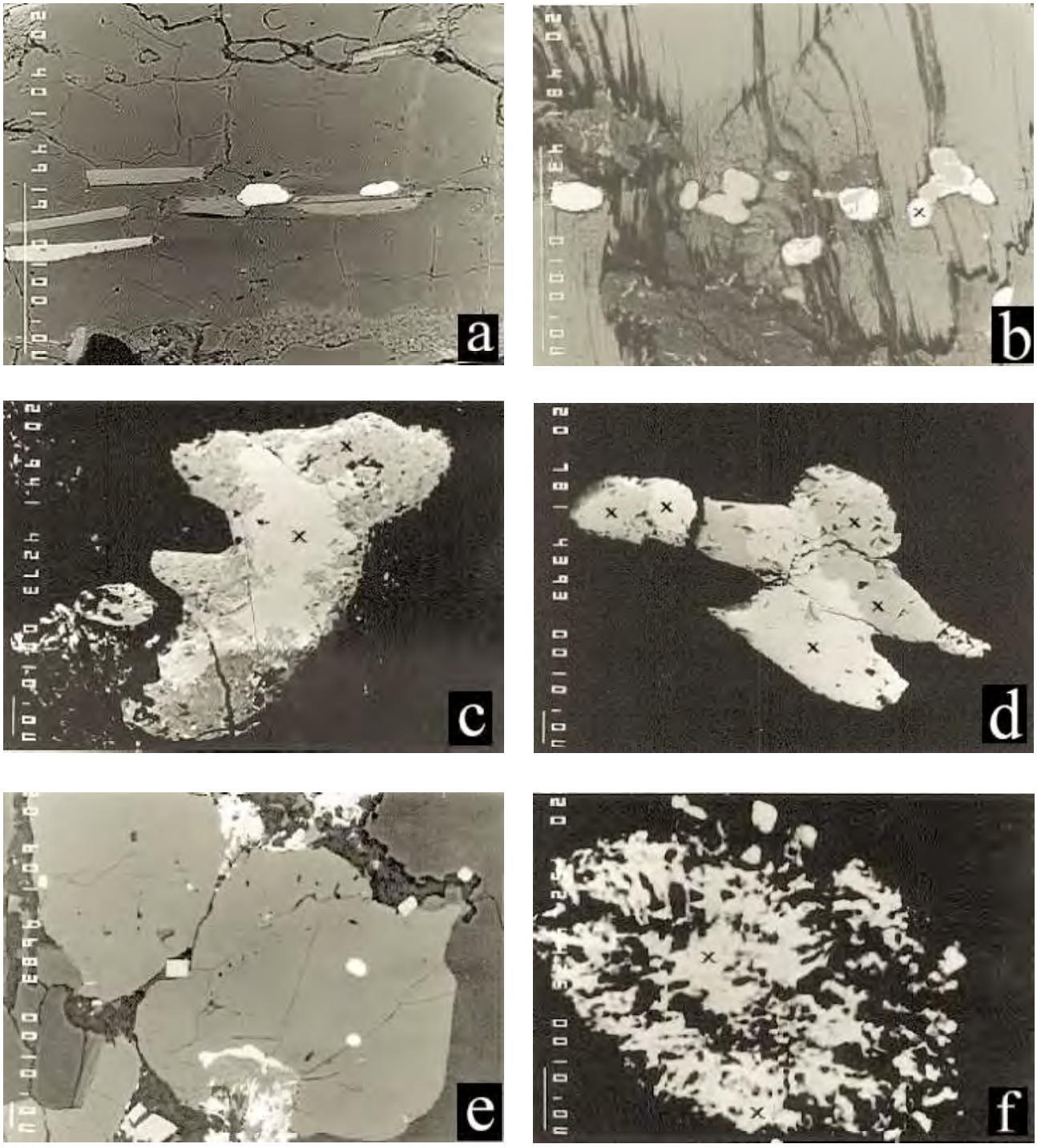

Fig. 4: Backscattered electron images. Locations of EMP-analyses are marked with „x".
a) Two idioblastic high-Y monazite-inclusions (white) in andalusite, together with biotite (medium grey) and ilmenite (bright grey) defining an older schistosity; Bt-And-Sil schist NM93-114 (ÓKB series); Scale bar: 100 mm. **b)** Monazite (bright grey) probably overgrowing xenotime (medium grey), next to biotite (medium grey, cleavage); Bt-And-Sil schist NM93-97 (ÓKB series); Scale bar: 100 mm. **c)** Low-Y monazite (bright grey) being corroded and overgrown by typical grainy Type 1 rhabdophane (medium grey); Bt-And-Sil schist NM92-71 (ÓKB series); Scale bar: 10 mm. **d)** Low-Y monazite (white) together with Type 2 rhabdophane (medium grey) showing similar appearance, but different brightness, Bt-And-Sil schist NM93-128 (ÓKB series); Scale bar: 10 mm. **e)** Monazite inclusions (white, rounded) in large apatite (medium grey). Zircon (bright grey, rectangular) and Type 1 rhabdophane (white, irregular) can be found at the rim of the apatite grains; medium grained ortho-gneiss NM93-121 (Sopron series); Scale bar: 10 mm. **f)** Amoeboidal Type 1 rhabdophane cluster (white, irregular) probably representing a pseudomorph after a pre-existing mineral; Ms-Chl-Grt-Bt-mica schist NM92-59 (Sopron series); Scale bar: 10 mm.

Sample NM92-6 contains numerous clusters of small Type 1 rhabdophane grains. They often seem to replace former mineral grains. No monazite or xenotime was found in this sample.

Garnet-biotite gneiss
Sample NM93-136 contains monazite and Type 1 rhabdophane but neither xenotime nor Type 2 rhabdophane. Most of the monazite grains are smaller than 10 μm. All are corroded, even those which are enclosed in biotite, garnet or ilmenite, and they often show rims of Type 1 rhabdophane. Their Y-content is low and their chemistry is comparable with other monazites with slightly stronger REE-concentration variations. Type 1 rhabdophane commonly appears at the rim or together with monazite, but also as independent grains. Two analyses of Type 1 rhabdophane show rather different compositions.

Sopron Series

Muscovite-chlorite-garnet schist
Monazite is very rare, xenotime is totally absent, and in one sample (NM92-22) Cl-apatite was found (Tab. 2). In NM92-7 there is one sector-zoned grain enclosed in quartz, with variable Y-content. In NM92-59 two monazite inclusions were found in two different garnet crystals, with similar compositions, one showing a rhabdophane rim.
Rhabdophane is present in all samples (Tab. 2). Type 1 rhabdophane in clusters of small grains and high Ca-content is relatively abundant in NM92-18. One 10 μm large grain with very high Th, Ca and Y-content is interpreted as brockite. NM92-59 contains comparatively many Type 1 rhabdophane grains, which often appear as pseudomorphs after a former mineral (Fig. 4f). In this sample, numerous analyses of Type 1 rhabdophane gave relative uniform compositions (Tab. 4) and oxide totals between 90.8 - 95.5 wt.%.
Abundant Type 2 rhabdophane forming 10 - 100 μm size irregular shaped grains was found in sample NM92-22. They have 94.1 - 95.4 wt.% oxide totals, even when enclosed in garnet.

Medium- and coarse-grained orthogneisses
None of the four examined samples (NM93-82, NM93-94, NM93-111 and NM93-121) contains monazite or xenotime greater than 10 μm in size.
Sample NM93-121 contains very little monazite, which are smaller than 10 μm, and enclosed in apatite, showing pronounced negative Eu-anomalies. The biggest one, shown in Fig. 4e is *c*. 7 μm long, with an oxide total of 97.6 wt.%. Smaller grains range between 95.4 to 96.9 wt.% (Tab. 3). Despite these low oxide totals, they are thought to represent monazite, because their compositions differ from that of rhabdophane in the same sample. The low oxide totals and high Ca-contents may be an artifact of their small size.
Type 1 Rhabdophane forms clusters of small grains in three gneiss samples (Tab. 2). They often have the appearance of pseudomorphs, and in places are attached to the boundaries of apatite (Fig. 4e). The Ca and Y-contents are relatively high, with variable Th (Tab. 4).

Muscovite-leuchtenbergite schist and kyanite-leuchtenbergite quartzite
The muscovite-leuchtenbergite-schist of sample NM93-85 contains many monazites, few xenotime, some Cl-apatite and one florencite grain(s). Monazite grains can be idioblastic, rounded or resorbed and in places zoned. Their compositions vary, with oxide totals between 98.5 and 99.6 wt.%. Four of the 7 analyses show strongly negative Eu-anomalies (Eu/Eu* ≤ 0.35), including the rim of a zoned grain.
The kyanite-leuchtenbergite quartzite of NM93-89 comprises less monazite and more xenotime and just some apatite containing Cl (Tab. 1). The monazite grains are rounded and form small groups. None of the leuchtenbergite-bearing rocks contain rhabdophane.

5. Discussion

Monazite is one of the most highly resistant minerals, during weathering, sedimentary transport, and metamorphism and therefore the biggest ore deposits are placer deposits (MARIANO 1989). It may survive, at least partly, during relatively high-grade metamorphism, although the exact stability limits are not known yet. SUZUKI et al. (1994) found detrital monazite grains in andalusite-sillimanite paragneisses (620 °C) and in sillimanite-orthoclase (680 °C) parageneses having preserved their pre-metamorphic age. SUZUKI & ADACHI (1994) dated monazite in paragneisses of the upper amphibolite facies, with different core and rim ages. WATT (1995) found corroded monazite in partly melted granulite at 800 °C, 0.6 GPa and water-undersaturated conditions, with their core retaining the original compositions. MONTEL et al. (1996) identified two monazite generations in gneiss inclusion of granite, and 3 generations in some polymetamorphic rocks.
On the other hand, FINGER et al. (1998) carefully documented the partial transformation of magmatic monazite in granitoid rocks to apatite, allanite and epidote during amphibolite facies metamorphism, at about 550-600 °C and 0.5-0.6 Gpa. Partial breakdown of monazite to apatite, was described by LANZIROTTI & HANSON (1996) in metapelites metamorphosed between 400 - 600 °C at 0.7 - 0.9 GPa, and by POITRASSON et al. (1996) in granites chloritised at 284 °C. Hydrothermal alteration of monazite has been illustrated by CESBRON (1989), with several examples.
The solubility of REE-phosphates has been studied by LIU & BYRNE (1997) at 25 °C, in highly acidic (pH = 1) hydrous solutions. According to their results, the solubility decreases from La to Pr and increases from Sm to Lu. The solubility of Y is nearly equivalent with Ho, both having similar ionic radii.
Monazite in the biotite-andalusite-sillimanite schists of the ÓKB Series are often enclosed in andalusite, in biotite, or can be found at the boundaries of these minerals; sometimes biotite is enclosed or intercalated. These textures suggest that the majority of these monazites have been formed before and/or during the andalusite forming metamorphic event.
The occurrence of high-Y and low-Y monazite with a well-defined gap in the Y-contents between the two groups is characteristic for the mica schists of the ÓKB Series (Fig.

5a and b). Except for NM93-97 containing both high- and low-Y monazite, the variations of the Y_2O_3 contents within each sample are smaller than in the prograde metamorphic rock series of FRANZ et al. (1996) and HEINRICH et al. (1997). The high-Y monazites are also enriched in other HREE compared with the values of low-Y monazites. In the Hungarian part of the crystalline, at Óbrennberg and Vöröshíd, the monazites in the mica schists of the ÓKB Series show similar division into two groups, with similar limits, except one sample in which the Y contents of the monazite grains varied continuously between the two groups (NAGY & ÁRKAI 1999).

HREE, i.e. the coexistence between monazite and xenotime was not maintained.

Compared with the abundance of monazite in the mica schists in the ÓKB Series, the mica schists of the Sopron Series contain only a few monazites and xenotime is missing totally. In NM92-59 monazite grains are only preserved as inclusions in garnet. Possibly existing monazite and xenotime, not armoured by other minerals, may have been transformed to rhabdophane during Alpine metamorphic processes. The increased fluid activity and intense deformation might have caused the destruction of monazite in the Sopron Series. The high differences in monazite

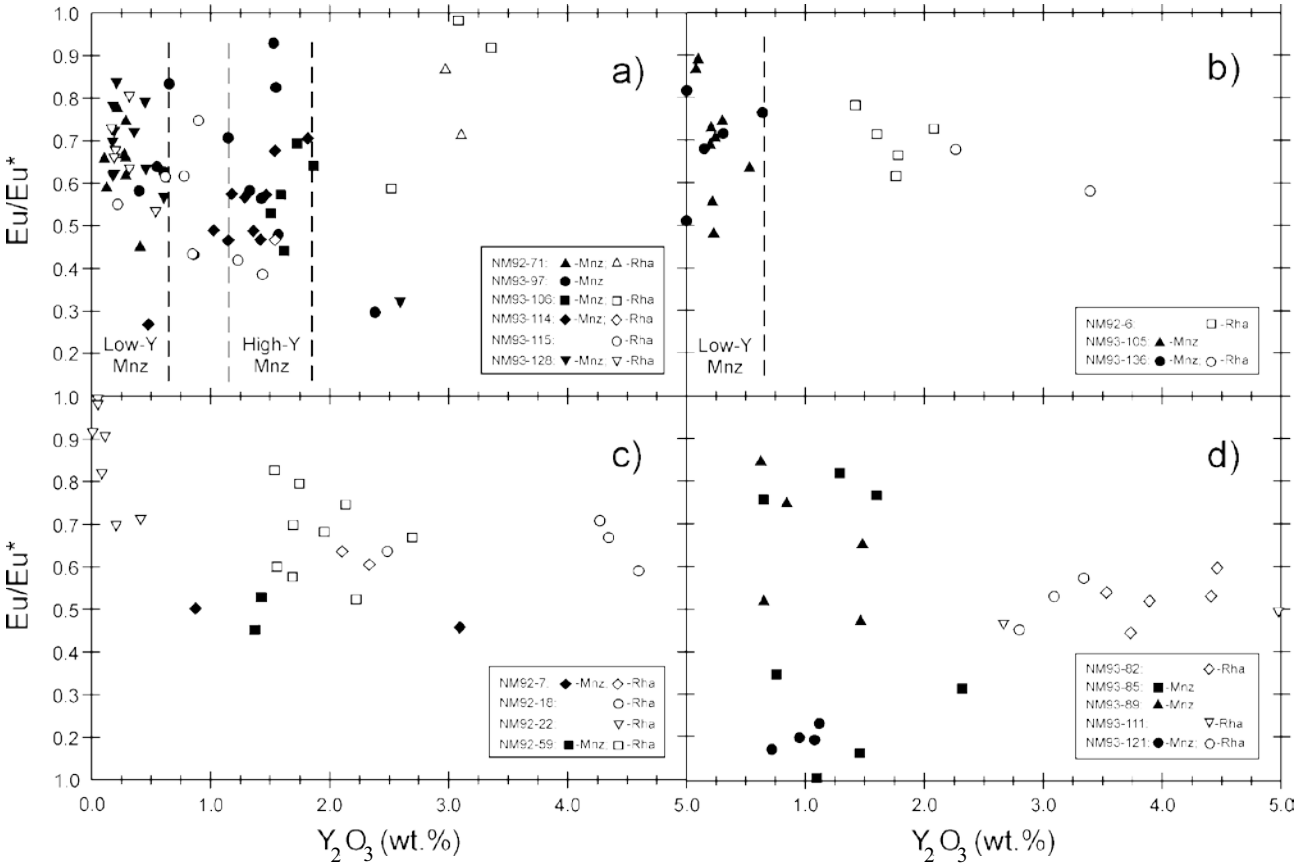

Fig. 5: Eu-anomaly *vs.* Y_2O_3-contents of monazite and rhabdophane. **a)** Bt-And-Sil schists (ÓKB Series). **b)** Chl-Ser-Grt schists (ÓKB Series). **c)** Mica schists (Sopron Series). **d)** Orthoneisses and Lbg-containing rocks (Sopron Series).

The differences in Y_2O_3 contents indicate that the monazite formation happened mainly in at least two different metamorphic events. Based on the experiences of FRANZ et al. (1996) and HEINRICH et al. (1997), and experiments of GRATZ & HEINRICH (1997, 1998) on the temperature/pressure dependency of the REE-chemistry of monazite coexisting with xenotime, monazite of the high-Y group formed under higher grade metamorphic conditions than the low-Y monazites. Due to the textural position of both, high- and low-Y monazite, included in andalusite as well as outside of andalusite, the time relation of both types remains unclear. The zoned grain in sample NM93-97 with the higher Y content in the centre would indicate that the higher-grade monazite is older than the lower T and/or P monazite. Another possibility is that, in the younger monazite-forming event, the REE-supplying medium was depleted in Y and

abundances found in the chlorite-sericite-garnet schists (NM92-6; NM93-105), which represent lithologies of the lowermost part of the ÓKB Series, might indicate local differences in the above mentioned factors.

Monazite is absent from most of the orthogneisses. In the medium-grained orthogneiss of sample NM93-121, only a few small monazite inclusions in apatite, which are probably of magmatic origin, are preserved. The lack of monazite in the meta-granitoid rocks (Tab. 1 and 2), except those armoured by minerals with low intracrystalline diffusion coefficients can be explained by the low stability of monazite in granitoid rocks during amphibolite facies metamorphism (FINGER et al. 1998 and references therein).

The leuchtenbergite-containing rocks in this area are strongly altered by Alpine deformation and metasomatism (HUBER 1993, DEMÉNY et al. 1997). The metasomatism

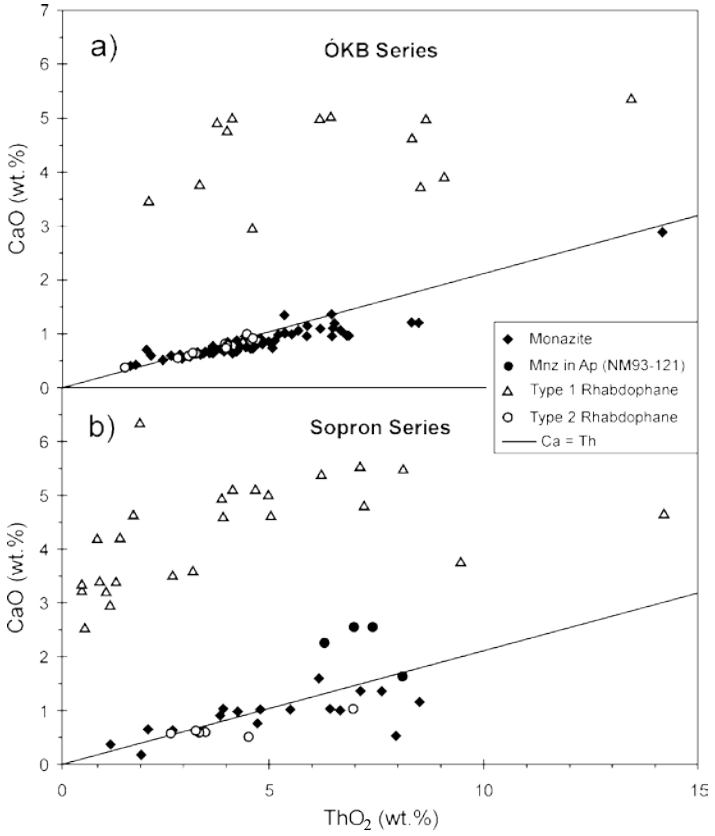

Fig. 6: Diagramm CaO *vs.* ThO_2 of all analyses on monazite and rhabdophane.
a) ÓKB Series.
b) Sopron Series.
Note the high Ca contents of Type 1 rhabdophane in both series and the strong scatter of monazite data points in the Sopron Series.

caused a strong depletion of the whole-rock composition in alkalies and Fe but enrichment in Mg and H_2O. The presence of Cl-apatite and florencite in these samples, as well as the chemistry of the outer rim of the zoned monazite in NM93-85, is probably related to these metasomatic processes. While it is very likely that leucophyllites (e.g. sample NM93-85) originated from highly sheared meta-granititic rocks, the protolith of the leuchtenbergite-kyanite-quartzite of NM93-89 is not certain. The investigated leucophyllite clearly contains more monazite than any of the investigated granitoids in the Sopron Hill, therefore its protolith may have been unusually rich in REE and/or REE have migrated from the surrounding rocks during metasomatic processes.
Most of the monazites have moderate negative Eu-anomalies, with Eu/Eu* = 0.40 - 0.95 (Fig. 5). Strongly negative anomalies with Eu/Eu* < 0.35 were observed only in few cases: (i) two „atypical analyses" (i.e. having Y-values not within the limits of high-Y- or low-Y monazites of the same rock sample) in Bt-And-Sil schists (NM93-97, NM93-114); (ii) small monazite inclusions in magmatic apatite in a medium-grained orthogneiss (NM93-121), which are very similar with those described in NAGY & ÁRKAI (1999); and (iii) monazite in the leucophyllite (NM93-85).
Up to now, only LANZIROTTI & HANSON (1996) have reported Eu-anomaly variations in two monazite populations having different metamorphic histories. Keeping in mind the multitude of different lithologies, the pronounced variations of the Eu-anomaly observed in the rocks of the Sopron hills are not surprising. Conversely, variations of this value within single samples may be interpreted by different origins (magmatic/metamorphic) or by growth during different metamorphic events.

Rhabdophane: Type 1 rhabdophane is rather widespread, in both the ÓKB Series and the Sopron Series. It is made of small grains, showing an appearance similar to rhabdophane described by BANFIELD & EGGLETON (1989). In the Sopron Hills, they occur in different textural positions. They are found either at the rim of monazite (Fig. 4c) or attached to or growing on the surface of apatite (Fig. 4e), often forming pseudomorphs after older minerals (Fig. 4f). Chemically, it is characterised by its high Ca-content; additionally its Y and HREE contents are always higher than that of monazite in the same rock (Fig. 5). The oxide totals range between 88.0 - 95.5 wt.%.
Type 1 rhabdophane growing at the rim of monazite (Fig. 4c) is probably the product of monazite alteration. The chemical differences exclude simple weathering and in this example it is almost impossible even by selective leaching, to reach the measured composition of the rhabdophane deriving from monazite. Yttrium, HREE and Ca are presumed to have entered from a hydrous solution by the following reaction

$$\text{monazite} + (Y,HREE) + Ca + H_2O = \text{Type 1 rhabdophane} \quad (4)$$

In most cases, the occurrence of Type 1 rhabdophane is not related to grains of monazite or even their existence in the rock. This implies that this rhabdophane formed from hydrous REE fluids, or more probably from partial or total disintegration of pre-existing monazite and/or xenotime (and Ca-containing mineral). This is supported by the observation that in samples with much rhabdophane and rare monazite, xenotime is scarce, too (Tab. 2).
Type 2 rhabdophane has a very similar appearance to

monazite, in terms of crystal shape, size and composition. It was distinguished from monazite by having oxide total values between 93.6 and 97.0 wt.%. Type 2 rhabdophane was found with or without monazite, but never together with Type 1 rhabdophane, and only in particular mica schists (Tab. 2). In NM93-128, numerous monazite and Type 2 rhabdophane grains were found; some independent from each other, some of them in an intimate contact (Fig. 4d). The coexistence of monazite and Type 2 rhabdophane in NM93-128 suggests that monazite was partly altered to Type 2 rhabdophane by incorporating water.

No rhabdophane, neither Type 1 nor Type 2, was found in leuchtenbergite-bearing rocks, both in the Austrian and the Hungarian part of the Sopron Hills. It is worth noting that in the Hungarian part, Type 1 rhabdophane is less widespread in mica schists, and Type 2 rhabdophane has not been found. Just one single florencite has been found in the Austrian part, which also has been identified in more leuchtenbergite bearing rocks in the Hungarian part (Nagy & Árkai, 1999).

6. Conclusions

In the metamorphic rocks of the Sopron Hills accessory REE-minerals are widespread. The most common of these minerals are monazite, rhabdophane and xenotime, whereas allanite and florencite are rare. The two tectonic units in the Sopron Hills show remarkable differences in their accessory REE-mineral characteristics. The Sopron Series (Lower Austroalpine tectonic unit) is generally very poor in monazite and xenotime, whereas the Óbrennberg-Kaltes Bründl Series (?Middle Austroalpine tectonic unit) contains these minerals in abundance, reflecting differences in their metamorphic evolution and, probably, in the REE contents of their source rocks. The retrograde formation of rhabdophane seems to have consumed monazite and xenotime within the lithologies of the Sopron Series, but affected the members ÓKB Series to a smaller degree, depending on the intensity of the Alpine metamorphic overprint.

In the schists of the ÓKB Series, monazites within a single sample show rather similar compositions, despite their different textural positions, but commonly have different Y-values between different samples of the same lithology. We suppose that local variations of the bulk rock composition controlled the monazite chemistry, rather than different P/T conditions during metamorphism.

The ThO_2 content of monazite varies within samples, sometimes even within one grain. CaO changes in a linear relationship with ThO_2 (Fig. 6b), nearly according to the reaction 2REE = Th + Ca, maintaining electric charge balance of the brabantite substitution.

The two different types of rhabdophane were never seen together in a single sample, indicating their different growth conditions during Alpine retrograde metamorphism. Whereas Type 2 rhabdophane seems to represent a simple hydration of monazite, with only minor chemical changes, the formation of Type 1 rhabdophane involved not only monazite and H_2O, but also xenotime, pointing to mobility of some rare earth elements.

Acknowledgements

ED thanks B. Grasemann for all kind of support. R. Berka and R. Schuster contributed many fruitful discussions on the regional geology. Abundant comments by H. Rice are much appreciated and improved both content and style. The final version benefited greatly from comments by F. Koller, H. Frimmel and R. Scheepers. This work has been financially supported by the Hungarian National Science Found (OTKA) program No. T015993.

References

Akers, W.T., Grove, M., Harrison, T.M. & Ryerson, F.J. (1993): The instability of rhabdophane and its unimportance in monazite paragenesis. - Chem. Geol., **110**: 169-176, Amsterdam.

Banfield, J.F. & Eggleton, R.A. (1989): Apatite replacement and rare earth mobilization, fractionation, and fixation during weathering. - Clays Clay Miner., **37**: 113-127, Oxford.

Balogh, K. & Dunkl, I. (1998): K-Ar and Ar-Ar dating of the Sopron Mts., Eastern Alps, Hungary. - 16th CBGA Congr., Abstr. Vol., 58, Vienna.

Berka, R., Schmidt, K., Schuster, R. & Frank, W. (1998): Hercynian- and Permian metamorphism in the eastern part of the Austroalpine basement (Eastern Alps). - Mitt. Österr. Miner. Ges., **143**: 242-245, Wien.

Bernhard, F., Finger, F., Schitter, F., Berka, R. & Schuster, R. (1998): Electron microprobe ages of monazite and xenotime from the Austroalpine basement units of the Fischbacher Alpen, Styria, Austria. - Mitt. Österr. Miner. Ges., **143**: 246-248, Wien.

Bowles, J.F.W. & Morgan, D.J. (1984): The composition of rhabdophane. - Miner. Mag., **48**: 146-148, London.

Braun, J.-J., Pagel, M., Muller, J.-P., Bilong, P., Michard, A. & Guillet, B. (1990): Cerium anomalies in lateritic profile. - Geochim. Cosmochim. Acta, **54**: 781-795, London.

Burt, D.M. (1989): Compositional and phase relations among rare earth element minerals. - (In: Lipin BR, McKay GA (eds) Geochemistry and Mineralogy of Rare Earth Elements), Rev. Miner., **21**: 259-307, Washington.

Cesbron, F.P. (1989): Mineralogy of the rare-earth elements. - (In: Möller, P., Cerný, P. & Saupé, F. (eds.): Lanthanides, Tantalum and Niobium), 3-26, (Springer) Berlin.

Clark, A.M. (1984): Mineralogy of the rare earth elements. - (In: Henderson, P. (ed.): Rare Earth Element Geochemistry), 33-54, (Elsevier) Amsterdam.

Demény, A., Sharp, Z.D. & Pfeifer, H.-R. (1997): Mg-metasomatism and formation conditions of Mg-chlorite-muscovite- quartzphyllites (leucophyllites) of the Eastern Alps (W. Hungary) and their relations to Alpine whiteschists. - Contr. Miner. Petrol., **128**: 247-260, Berlin.

Draganits, E. (1996): Kristallingeologische Neubearbeitung des südlichen Ödenburger Gebirges, Burgenland (Österreich). - 1-151, Unveröff. Dipl. Arb., Nat. Wiss. Fak. Univ. Wien.

Draganits, E (1998): Seriengliederung im Kristallin des südlichen Ödenburger Gebirges (Burgenland) und deren Stellung zum Unterostalpin am Alpenostrand. - Jb. Geol. Bundesanstalt, **141**: 113-146, Wien.

Drake, M.J. & Weill, D.F. (1972): New rare earth element standards for electron microprobe analysis. - Chem. Geol., **10**: 179-181, Amsterdam.

Faryad, S.W. & Hoinkes, G. (1998): Correlation of metamorphic P-T conditions between basement rocks in the Austro-Alpine units east from the Tauern Window and in the eastern sector of the western Carpathians. - 159, 16th CBGA Congr., Abstr. Vol., Vienna.

Fazekas, V., Kósa, L. & Selmeczi, B. (1975): Rare earth mineralization in the crystalline schists of the Sopron Moun-

tains. - Földtani Közlöny, **105**: 297-308 (in Hungarian with English abstract), Budapest.

FINGER, F., BROSKA, I., ROBERTS, M. & SCHERMAIER A (1998): Replacement of primary monazite by apatit-allanite-epidote coronas in an amphibolite facies granite gneiss from the eastern Alps. - Amer. Miner., **83**: 248-258, Washington.

FRANZ, G., ANDREHS, G. & RHEDE, D. (1996): Crystal chemistry of monazite and xenotime from Saxothuringian-Moldanubian metapelites, NE Bavaria, Germany. - Europ. J. Miner., **8**: 1097-1118, Stuttgart.

GRATZ, R. & HEINRICH, W. (1997): Monazite-xenotime thermobarometry: Experimental calibration of the miscibility gap in the binary system $CePO_4$-YPO_4. - Amer. Miner., **82**: 772-780, Washington.

GRATZ, R. & HEINRICH, W. (1998): Monazite-xenotime thermobarometry: III. Experimental calibration of the partitioning of gadolinium between monazite and xenotime. - Eur. J. Miner., **10**: 579-588, Stuttgart.

GRAUCH, R.I. (1989): Rare earth elements in metamorphic rocks. - (In: LIPIN, B.R. & MCKAY, G.A. (eds.): Geochemistry and Mineralogy of Rare Earth Elements) - Rev. Miner., **21**: 147-167, Washington.

HEINRICH, W., ANDREHS, G. & FRANZ, G. (1997): Monazite-xenotime miscibility gap thermometry. An empirical calibration. - J. Metam. Geol., **15**: 3-16, Oxford.

HENDERSON, P. (1984): General geochemical properties and abundances of the rare earth elements. - (In: HENDERSON, P. (ed.): Rare Earth Element Geochemistry), 1-32, (Elsevier) Amsterdam.

HIKICHI, Y., YU, C.F., MIYAMOTO, M. & OKADA, S. (1991): Mechanical conversion of rhabdophane type RPO_4nH_2O (R=La, Ce, Pr, Nd, or Sm, n 1/2) to the monazite type analogues. - Miner. J., **15**: 349-355, Tokyo.

HUBER, M. (1993): Bildung und geotektonische Bedeutung von Scherzonen (Leukophylliten) am Alpenostrand. - 1-136, Unveröff. Dissertation, Institut für Geowissenschaften, Univ. Leoben.

HUGHES, J.M., FOORD, E.E., HUBBARD, M.A. & NI, Y. (1995): The crystal structure of cheralite-(Ce), (LREE,Ca,Th,U)(P,Si)O , a monazite-group mineral. - N. Jb. Miner. Monatshefte, **1995**: 344-350, Stuttgart.

JONES, A.P., WALL, F. & WILLIAMS, C.T. (1996): Rare Earth Minerals Chemistry, origin and ore deposits. - 1-372, (Chapman & Hall) London.

KIESL, W., WIESENEDER, H. & KLUGER, F. (1983): Untersuchungen des Vorkommens der Seltenen Erden und von Thorium in Gesteinen des unteraustroalpinen Kristallins des Semmering-Wechselfensterns. - Sitzungsber Österr Akad Wiss Mathem-Naturwiss Kl, Abt I, **192**/1-4: 1-20, Wien.

KISHÁZI, P. & IVANCSICS, J. (1985): Genetic petrology of the Sopron crystalline schist sequence. - Acta Geol. Hung., **28**/3-4: 191-213, Budapest.

KOLLER, F. & WIESENEDER, H. (1981): Gesteinsserien und Metamorphosen der Rechnitzer Serie im Burgenland und des Unterostalpins in der Oststeiermark. - Fortschr. Miner., **59**, Beih 2: 167-178, Stuttgart.

KRETZ, R. (1983): Symbols for rock-forming minerals. - Amer. Miner. **68**: 277-279, Washington.

LANZIROTTI, A. & HANSON, G.N. (1996): Geochronology and geochemistry of multiple generations of monazite from the Wepawaug Schist, Connecticut, USA – implications for monazite stability in metamorphic rocks. - Contrib. Miner. Petrol., **125**: 332-340, Berlin.

LELKES-FELVÁRI, G. & SASSI, F.P. (1984): Pre-alpine and alpine developments of the austridic basement in the Sopron area (Eastern Alps, Hungary). - Rend. Soc. Italiana Miner. Petrol., **39**: 593-612, Roma.

LIU, X. & BYRNE, R.H. (1997): Rare earth and yttrium phosphate solubilities in aqueous solution. - Geochim. Cosmochim. Acta, **61**: 1625-1633, London.

MARIANO, A.N. (1989): Economic geology of the rare earth elements. – (In: LIPIN, B.R. & MCKAY, G.A. (eds.): Geochemistry and Mineralogy of Rare Earth Elements), Rev. Miner., **21**: 309-337, Washington.

MONTEL, J.-M., FORET, S., VESCHAMBRE, M., NICOLLET, C. & PROVOST, A. (1996): Electron microprobe dating of monazite. - Chem. Geol., **131**: 37-53, Amsterdam.

MOONEY, R.C. (1950): X-ray diffraction study of cerous phosphate and related crystals I Hexagonal modification. - Acta Crystallographica, **3**: 337-340, Copenhagen.

NAGY, G. (1993): „Quick" method for REE mineral analysis by EPMA. - 94-96, International Conference on Rare Earth Minerals, London, 1-2 April 1993, London.

NAGY, G., ÁRKAI, P. (1999): Monazite in the metamorphic formations of the Sopron Hills, Eastern Alps, Hungary. - Földtani Közlöny, **129**, 267-303, Budapest (in Hung. with Engl. summary).

POITRASSON, F., CHENERY, S. & BLAND, D.J. (1996): Contrasted monazite hydrothermal alteration mechanisms and their geochemical implications. - Earth Planet. Sci. Lett., **145**: 79-96, Amsterdam.

PAN, Y. (1997): Zircon- and monazite-forming metamorphic reactions at Manitouwadge, Ontario. - Canad. Miner., **35**: 105-118, Ottawa.

SAWKA, W.N., BANFIELD, J.F. & CHAPPELL BW (1986): A waethering-related origin of widespread monazite in S-type granites. - Geochim. Cosmochim. Acta, **50**: 171-175, London.

SCHWINNER, R. (1935): Zur Geologie von Birkfeld. - Mitt. Naturwiss. Vereins Steiermark, **72**, 67-100, Graz.

SCHUSTER, R., SCHARBERT, S. & ABART, R. (1998): Permo-Triassic high temperature/low pressure metamorphism in Austroalpine basement units (Eastern Alps). - Mitt. Österr. Miner. Ges., **143**: 383-386, Wien.

STRUNZ, H. (1970): Mineralogische Tabellen. - 1-621, (Akademische Verlagsgesellschaft) Leipzig.

SUZUKI, K. & ADACHI, M. (1994): Middle Precambrian detrital monazite and zircon from the Hida gneiss on Oki-Dogo Island, Japan their origin and implications for the correlation of basement gneiss of Southwest Japan and Korea. - Tectonophysics, **235**: 277-292, Amsterdam.

SUZUKI, K., ADACHI, M. & KAJIZUKA, I. (1994): Electron microprobe observations of Pb diffusion in metamorphosed detrital monazites. - Earth Planet. Sci. Lett., **128**: 391-405, Amsterdam.

TAYLOR, S.R. & MCLENNAN, S.M. (1985): The Continental Crust: Its Composition and Evolution. - 1-312, (Blackwell) Oxford.

TÖRÖK, K. (1996): High-pressure/low-temperature metamorphism of the Kö-hegy gneiss, Sopron (W-Hungary); phengite barometry and fluid inclusions. - Europ. J. Miner., **8**: 917-925, Stuttgart.

VLASOV, K.A. (1964): Geochemistry, mineralogy and genetic types of rare element deposits. - Mineralogy of rare elements,Vol 2, 1-830, (Nauka) Moskow, (in Russ.).

WATT, G.R. (1995): High-thorium monazite-(Ce) formed during disequilibrium melting of metapelites under granulite-facies conditions. - Miner. Mag., **59**: 735-743, London.